Superconductor Science and Technology

PAPER

Integration of vertically-aligned carbon nanotubes with superconducting nanowire single photon detectors

IOP Publishing
Superconductor Science and Technology
Supercond. Sci. Technol. **37** (2024) 015005 (6pp)
https://doi.org/10.1088/1361-6668/ad0db3

Integration of vertically-aligned carbon nanotubes with superconducting nanowire single photon detectors

D S Rampini[1,2], C S Yung[1], B G Oripov[1,2], S Woods[1], J Lehman[1], S W Nam[1] and A N McCaughan[1,*]

[1] National Institute of Standards and Technology, Boulder, CO 80305, United States of America
[2] Department of Physics, University of Colorado, Boulder, CO 80309, United States of America

E-mail: adam.mccaughan@nist.gov

Received 23 June 2023, revised 11 October 2023
Accepted for publication 17 November 2023
Published 27 November 2023

Abstract
We report on initial fabrication efforts in the integration of superconducting nanowire single-photon detectors (SNSPDs) with vertically aligned carbon nanotubes (VACNTs) with the goal of creating a wideband single-photon detector. SNSPDs provide high detection efficiencies and low dark count rates, while the VACNTs are excellent broadband optical absorbers. Combining these technologies could potentially enable the development of highly sensitive and versatile optical sensors for a variety of applications, such as spectroscopy, optical communication, and imaging in light starved environments. We developed two fabrication processes for the integration of VACNTs on SNSPDs. The first involves capping the SNSPDs with a protective layer and growing the VACNTs directly above nanowires. Thermal and electrical characterizations of the devices demonstrated a degradation of the superconducting qualities of the SNSPDs. The second process involved suspending the SNSPDs on a thin membrane via a backside etch, where VACNTs were then grown on the backside of the membranes below the nanowires. The membrane style devices showed no degradation in the superconducting properties of the nanowires. Measurements of the membrane style devices before and after the VACNT growth display similar superconducting properties and photon count rates.

Keywords: SNSPD, VACNT, nanowire, cnt, carbon nanotube, growth, fabrication

1. Introduction

Superconducting nanowire single-photon detectors (SNSPD) are a type of single-photon detector that use superconducting nanowires to detect individual photons. These nanowires are typically made from superconducting thin films such as niobium nitride (NbN), molybdenum silicide (MoSi) or tungsten silicide (WSi). The nanowires are typically meandered into rectangular or circular pixels with a high fill factor and are generally 100–1000 nm wide with a film thickness of less than 10 nm. SNSPDs are one of the leading technologies in single photon detection due to several advantages over traditional single-photon detectors, including high detection efficiency, low dark count rate, low jitter, and ultra-fast response times [1, 2]. SNSPDs have been shown to have excellent detection properties from the UV [3, 4] to the mid-infrared [1], but typically to get high system detection efficiencies (⩾75%) an optical stack to the detector must be used to optimize the coupling of the incident light. As a result, these detectors usually only operate with high efficiencies at the specific wavelength of the narrowband optical stack. For example, a system detection efficiency of 98% has been achieved only between 1530–1540 nm where the optical stack was optimized [1].

* Author to whom any correspondence should be addressed.

One potentially complementary technology that has gained wide use in electronics and optics in the past few decades are carbon nanotubes (CNTs) due to their unique electrical, thermal and optical properties [5–8]. Of particular interest are vertically-aligned CNTs (VACNTs), which are CNTs that are grown in a vertical orientation, with their long axes perpendicular to the substrate on which they are grown. VACNTs are nearly ideal optical absorbers due to their exceptionally low reflectance over a broad wavelength range, with $>$99% absorption from 300 nm to 50 μm [9–12]. The absorption mechanism in CNTs is still a debated topic in the literature, however there is strong evidence that the optical properties are excitonic from experimental observations and theoretical findings of exciton-phonon complexes. These studies show the importance of phonons in the current understanding of excitation and recombination mechanisms in CNTs [13–15]. At the same time, the role of the photon-to-phonon downconversion process in SNSPDs has begun to be elucidated in the literature [16], and a number of recent demonstrations have shown that these nanowire detectors not only detect energy absorbed directly from photons, but are also sensitive to small amounts of thermal or athermal phonons [17–19]. Coupling VACNTs to SNSPDs could enable the creation of a broadband photodetector by using the VACNTs as wideband photon absorbers and thermally coupling the resulting nonequilibrium phonons through them to the SNSPDs. Unfortunately, just the integration of VACNTs with SNSPDs is a challenging problem. For instance, the iron-based seed layer used in the growth of VACNTs can diffuse, leading to ferromagnetic impurities in the superconducting thin film. In this work, we have established two fabrication processes for the incorporation of VACNTs on WSi SNSPDs by the addition of a capping layer or the use of an ultrathin membrane. Electrical measurements of the capping layer devices demonstrated a loss in superconductivity in the WSi thin film, whereas no disturbance in the superconducting properties is measured in the membrane style devices. Optical measurement comparisons of the membrane style devices with and without VACNTs indicate no significant thermal coupling between the VACNTs and SNSPDs–future work exploring the VACNT-SNSPD integration process will be crucial to practically demonstrating this coupling.

In the typical SNSPD detection process a photon is directly absorbed by the superconducting nanowire material, and the deposited photon energy disrupts the superconducting state of the nanowire in that localized region. In the presence of a large enough bias current density, this disruption causes the region to become a resistive hotspot and generates electrical output for readout. The ideal principle of operation of the coupled VACNT-SNSPD device would follow a similar scheme. When a photon is absorbed by a VACNT, the photon energy is converted into phonons in the nanotube. If we could couple the phonons efficiently from the nanotube to a nearby SNSPD and sufficient energy is transferred to the nanowire in a localized fashion, then a hotspot could be created in the nanowire much in the same way as a direct absorption of a photon. The exact phonon coupling mechanism between a VACNT and nearby superconductor is not well-understood at present, and so in this work we aim to take a first step at exploring this interaction. By first developing a robust fabrication process to integrate VACNTs with SNSPDs, we can then explore this interaction further, for instance by increasing the photon energy with shorter-wavelength photons, or minimizing the specific heat of the CNTs by growing them shorter.

2. Fabrication

The process of implementing VACNTs with SNSPDs presents some unique fabrication challenges. The VACNT growth process requires annealing at high temperatures (800 °C) and an iron seed layer that acts as a catalyst during the VACNT growth procedure. Annealing superconducting thin films can cause morphology changes that affect the superconducting properties of the film [20, 21] and ferromagnetic impurities are known to cause the degradation of superconductivity [22]. The high aspect ratio and fragile nature of VACNTs also limits the fabrication processes that can be done post VACNT growth [9] such as liquid processing, depositions, etc, and this requires the VACNT growth to be the last step in the fabrication procedure. With these challenges in mind, a working fabrication process that protects the superconducting layer must be found. We successfully developed two fabrication methods, a top-side and bottom-side fabrication procedure, that allowed us to grow VACNTs on top of SNSPDs without destroying superconducting properties of the SNSPDs. Critically, the SNSPDs were still capable of detecting photons absorbed directly into the superconducting material, however we cannot yet attribute any SNSPD detection to VACNT enhancement.

Our first method of integration was to protect the SNSPDs with a capping layer and then grow the VACNTs on top of the capping layer shown in figure 1(a). We began by fabricating the SNSPDs on a 150 nm thermal oxide silicon wafer. We deposited 4 nm of WSi via co-sputtering from separate W and Si targets, with sputtering powers of 100 and 180 W respectively, followed by a 2 nm aSi deposition *in-situ* to protect the superconducting layer from oxidizing. SNSPDs were then patterned via optical lithography and etched in an RIE using SF_6. Next, a 5 nm Ti and 80 nm Au evaporation and liftoff step was then completed to add wire bonding pads to the devices. Lastly, we sputtered 3 nm SiNx and 12 nm AlN and liftoff to complete the capping layer. For the VACNT growth, 2 nm of Fe was deposited on the capping layer to seed the VACNT growth. The wafer was then baked at 800 °C for 10 min in an ethylene (C_2H_4) atmosphere, resulting in VACNTs with a height of 70 um in the desired areas. All designs were made in Python using the phidl design package [23]. After initial measurements of these devices, we discovered that the superconducting properties of the WSi layer were depleted through measurements of the critical temperature and critical currents of the superconducting layer. This degradation was likely caused by Fe poisoning in the SNSPDs via the diffusion of Fe particles through the capping layer into the WSi film.

The second fabrication process found more success in preserving the superconductivity of the WSi SNSPDs. The main

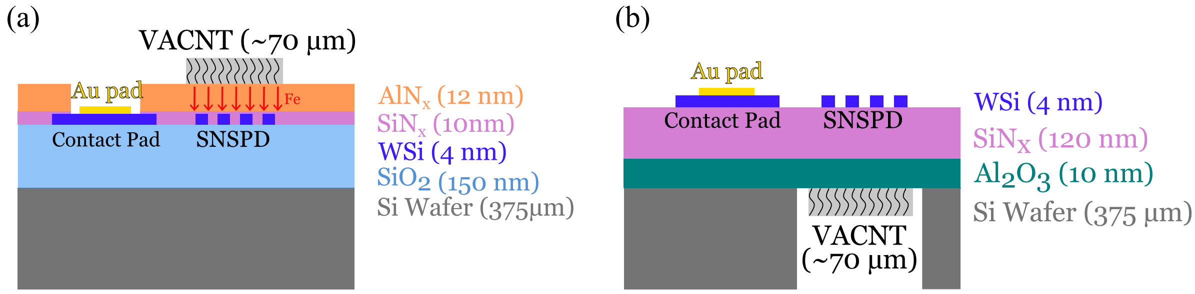

Figure 1. Cross-sectional view of the two fabrication processes for integrating VACNTs with SNSPDs. (a) Integrating VACNTs directly on the surface of the SNSPD, using a capping layer between them (b) Growing the VACNTs on the underside of a membrane-suspended SNSPD.

difference from the previous approach, seen in figure 1(b), is that the VACNTs are grown on the bottom of membrane style SNSPDs. We began this process by depositing 10 nm Al_2O_3 via atomic layer deposition (ALD) as an etch stop and 120 nm of SiNx as a capping layer via a plasma-enhanced chemical vapor (PECVD) deposition on a Si wafer. We then followed the same WSi deposition and Au pad liftoff method for the SNSPD previously described, however the SNSPDs were written via electron-beam lithography in order to reduce the feature sizes of the detectors from the previous iteration. Once the SNSPDs were fabricated, we etched the backside of the Si wafer via deep-reactive-ion-etching until the 10 nm Al_2O_3 etch stop layer was reached. Following the backside etch the same VACNT growth procedure was implemented on the backside of the membranes. This resulted in WSi SNSPDs suspended on a 10 nm Al_2O_3 plus 120 nm SiN_x membrane with 70 nm VACNTs on the backside of the membrane. Optical images and SEM images of the membrane style devices before and after VACNT growth are shown in figure 2.

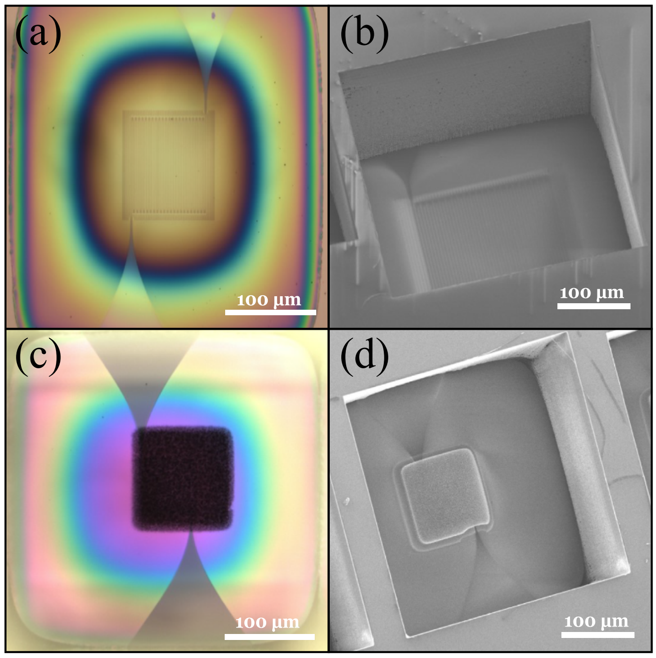

Figure 2. Optical and scanning-electron microscope (SEM) images of the membrane-style devices. (a) Optical image before VACNT growth, (b) SEM before VACNT growth, (c) optical image after VACNT growth and (d) SEM after VACNT growth.

3. Experimental results

After fabrication, we characterized the integrated detectors through a series of electrical and optical tests. Three types of measurements were taken on 150 nm wide meandered membrane style SNSPDs with a 50% fill-factor and a detection area of $16 \times 16\,\mu$m. First, to ensure the survivability of the superconductivity of the WSi post-VACNT growth we measured the critical temperature of two SNSPDs from different chips diced from the same wafer. The resistivity versus temperature measurements were made using a four-wire resistance measurement on one of the SNSPDs and varying the temperature between 1.7 K and 6 K. The chips were electrically connected to the device's contact pads with aluminum wire bonds and were attached to the sample holder using rubber cement. The temperature was swept at a rate of 0.5 K $\min^{-1}$ while continuously measuring the resistance. The results are shown in figure 3, plotting the normalized resistance of each device vs temperature. The pre-VACNT and post-VACNT devices have a critical temperature of 3.5 K, with the curves overlapping almost perfectly.

The next two measurements, IV curves and photon count rate (PCR) of the SNSPDs, were taken in a cryostat at a base temperature of 800 mK. The sample chip was mounted on a PCB connected to an aluminum block that is attached to the 800 mK stage to act as a heatsink. The devices were wirebonded to pads on the PCB, the pads were connected to an SMA connector where 50 Ω SMA cables connect to room temperature electronics. One key difference from the critical temperature measurements is that the IV and PCR measurements were taken on the same chip after the VACNT growth procedure. These measurements compared a membrane-style SNSPD and a membrane-style SNSPD with backside VACNT growth. The IV curves were taken at a ramp rate of 2 mA s^{-1}. In our set-up we used an arbitrary waveform generator to generate the current ramp, a 2 GHz oscilloscope, two 1.9 MHz lowpass filters and a 10 kΩ bias resistor. The IV curves for the membrane SNSPD and membrane SNSPD with backside VACNT growth are shown in figure 4 with critical currents of 11.2 uA and 11.5 uA respectively.

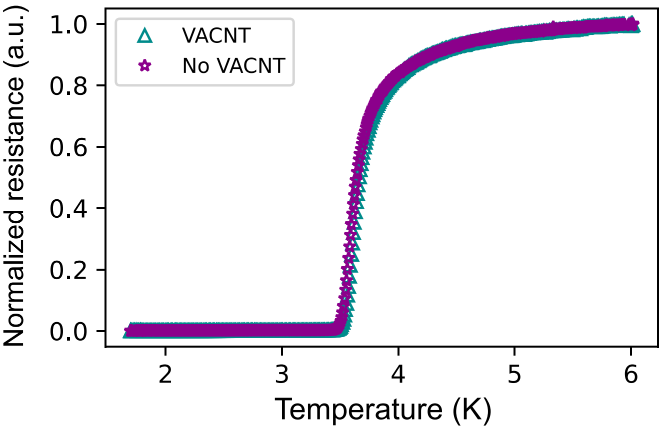

Figure 3. T_c measurement of a membrane-style device, showing that the VACNT growth process does not reduce the critical temperature of the SNSPD film. Plotting measured normalized resistance as a function of temperature before VANCT growth (purple) and after VACNT growth (blue).

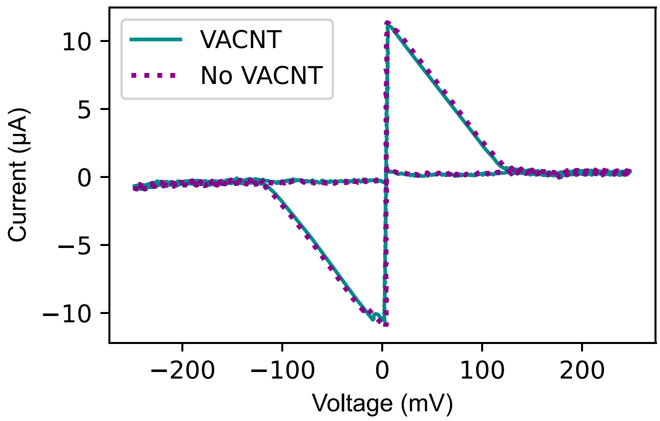

Figure 4. IV curves of membrane style SNSPDs with VACNTs (blue) and without (purple), showing that VACNTs could be integrated without reducing the current-carrying capacity of the SNSPD.

To characterize the PCRs of the two devices we used a 980 nm laser source connected to an optical attenuator that was connected to a fiber feedthrough in the cryostat. We flood illuminated the sample from a distance of approximately 5 cm, generating a Gaussian spot on the sample with a diameter of approximately 1 cm. For the PCR measurements we biased the device with a low-noise DC voltage source applied to a 10 kΩ bias resistor connected to the DC port of a bias-tee. The SNSPDs were connected to the RF+DC port of the bias-tee and the RF output was connected to two low noise amplifiers with a total gain of 46 dB. The amplifiers' output was connected to a counter where the SNSPD pulses were detected. We used a 100 mV trigger and a gate time of 500 ms for all of the PCR measurements. The bias current to the devices was calculated by measuring the voltage drop across the bias resistor and dividing this value by the bias resistance. All the electronics resided at room temperature. In order to gain insight into whether the VACNTs were accomplishing the task of creating clicks in the SNSPDs after photon absorption we measured the devices by illuminating the frontside (SNSPD side) and backside (VACNT side) during two separate cooldowns. The PCR results for both cooldowns are shown in figure 5.

4. Discussion

The frontside measurements, as well as the T_c and IV plots, demonstrate that there is negligible loss in superconductivity or SNSPD performance caused by the VACNT growth on the backside of the membranes. In figure 5(a), it is apparent from frontside PCR curves of VANCT and non-VACNT devices demonstrate similar count rates and plateau regimes, indicating similar performance of the devices. However, the backside illumination PCR results show a steep decrease in counts between the two devices, from 1.03×10^5 counts per second (cps) for the membrane style SNSPD to 20 cps for the membrane style SNSPD with backside VACNT growth. From these results it is clear that the photons absorbed by the VACNT few, if any, clicks in the SNSPD. The 20 cps measured are likely due to one of three scenarios: (1) that VACNTs are not perfect absorbers, and some photons do get through the VACNT forest and generate counts because they are absorbed directly in the superconducting material, (2) due to the imperfect flood-illumination setup, there was some amount of light reflected behind the sample that was then absorbed on the device frontside, or (3) a small fraction of the photons absorbed in the VACNT forest are in fact coupling to the SNSPD and generating counts. Similar results were also measured at 785 nm and 1550 nm on the same devices with large decreases in countrates during backside illumination.

A point of interest in the PCR measurements are the dark count rates observed. In both the frontside and backside measurements the dark count rates cut off at a higher bias current than the PCRs. This cutoff is due to the SNSPDs residing on very thin membranes. During the PCR measurements the heat produced by photon absorption events in the nanowire can only travel laterally through the membrane before being able to diffuse into the substrate. In this scenario the heat is more concentrated than with a regular style device where the heat can diffuse directly into the substrate. This causes the membrane style devices to switch to the normal state at a smaller bias current when illuminated during the PCR measurements, whereas the dark counts are able to reach a higher bias current due to the lack of heat concentration. A decrease in dark count rates is also observed in the VACNT devices, an observation that requires further investigation in the next measurements and iterations of these devices. Regardless of the exact cause, the large loss of counts indicates that there is little to no transduction from a photon absorption event in a VACNT to a hotspot creation in the nanowires. There are multiple possible reasons for this behavior. First, the 70 um tall VACNTs were much taller than strictly necessary, potentially operating as a phonon heat sink before the photon energy reached the membrane and subsequent nanowire layer. An alternative explanation is that even though the VACNTs are single, vertically-aligned entities they may touch or otherwise be in

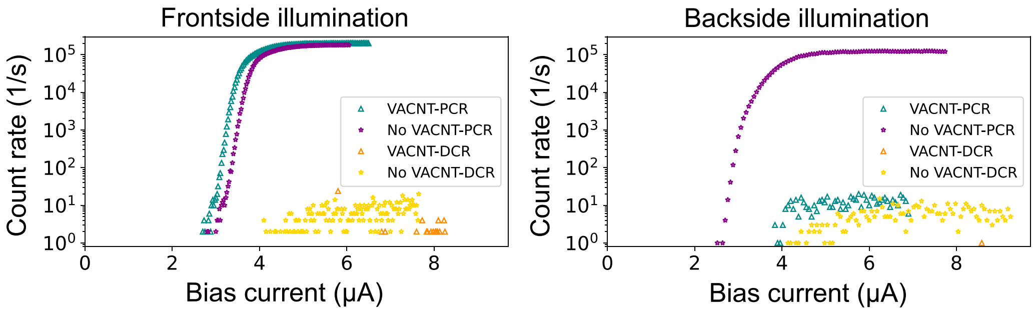

Figure 5. Photon count rates and dark count rates of membrane-style devices. PCR measurements taken using flood illumination at 980 nm. Measured same devices in two separate cooldowns. (left) frontside illumination and (right) backside illumination.

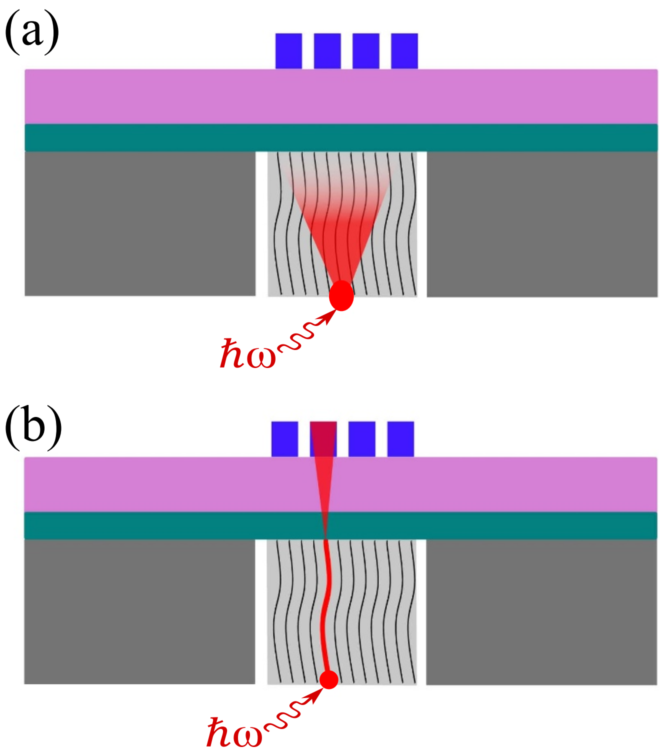

Figure 6. Potential heating dynamics in membrane style devices. (a) Phonons generated from photon absorption in a VACNT diffuse throughout VACNT forest volume. Once phonons reach the capping layer the energy is not localized enough to produce a hot-spot in the nanowire. (b) A single nanotube carries the deposited energy to the surface of the substrate. These phonons then travel through the capping layer to the nanowire in a localized fashion and induce a hot-spot in the nanowire. It must be noted that the thermal transport properties of carbon nanotubes will also depend on crystallinity, defects, temperature, density and temperature-dependent electron phonon mobility [24].

contact with other VACNTs. These points of contact to other nanotubes could act as avenues for the phonons to diffuse laterally, instead of the energy from the photon absorption event traveling along one single VANCT; this idea is summarized in figure 6.

There are practical issues in the measuring set-up of these devices that are worth noting to the reader. For instance, the small thickness of the membranes make these devices extremely fragile. The surface pressure caused on the devices when wire bonding can lead to the destruction of the membranes. Measuring the devices between VACNT growth also caused purple plague, caused by the Al from the wire-bonds on the Au pads [25], during the high temperature annealing process. The annealing creates a gold-aluminum intermetallic compound that degrades the pads and makes it very difficult to re-wirebond to the same device post VACNT growth. These issues could be fixed by using probe tips as electrical contacts or sputtering a different metal for the device contact pads. There are also practical matters affecting the reproducibility of the devices. For instance, the VACNT growth process is difficult to control, and the height and density of the VACNTs can depend on many factors including the precise layout, positions, and sizes of the VACNT catalyst layer.

There is a necessity to quantify these hypotheses in future iterations of these devices. Some potential avenues for improvement and further quantification include smaller VACNT islands grown along the widths of the nanowires via electron beam lithography, decreasing VACNT height, decreasing membrane thickness, and exploring new capping layer oxides and thicknesses to better protect the nanowires from ferromagnetic impurities depleting the superconductivity of the WSi thin film.

5. Conclusion

We have developed a working fabrication process to incorporate VACNTs with WSi SNSPDs. Two fabrication approaches were completed and studied. The initial capping layer method resulted in the degradation of superconductivity in the WSi thin film, likely due to the diffusion of ferromagnetic Fe particles during the annealing process of the VACNT growth. The latter membrane style approach found more success and did not affect the superconducting properties of the WSi layer. Experimental results of the membrane style devices indicate no coupling between the VACNTs and SNSPDs; this suggests that photon absorption events do not generate detectable hotspots in the nanowires. However, the development of these fabrication approaches are an important first step towards integrating these valuable technologies. Future work will include optimizing the fabrication processes in order to localize the dissipated heat in the VACNTs and simulations to gain insight into the photon absorption process in the VACNTs and the coupling of the phonon energy to the SNSPDs. This research was funded by NIST (https://ror.org/05xpvk416) and the University Colorado Boulder (https://ror.org/02ttsq026).

Data availability statement

All data that support the findings of this study are included within the article (and any supplementary files).

ORCID iDs

C S Yung https://orcid.org/0000-0002-7912-6591
B G Oripov https://orcid.org/0000-0002-6626-2076
S Woods https://orcid.org/0000-0002-1037-3025
A N McCaughan https://orcid.org/0000-0002-8553-6474

References

[1] Reddy D V, Nerem R R, Woo Nam S, Mirin R P and Verma V B 2020 Superconducting nanowire single-photon detectors with 98% system detection efficiency at 1550 nm *Optica* **7** 1649
[2] Verma V B, Korzh B, Bussières F, Horansky R D, Lita A E, Marsili F, Shaw M D, Zbinden H, Mirin R P and Nam S W 2014 High-efficiency WSi superconducting nanowire single-photon detectors operating at 2.5 K *Appl. Phys. Lett.* **105** 122601
[3] Wollman E E *et al* 2017 UV superconducting nanowire single-photon detectors with high efficiency, low noise and 4 K operating temperature *Opt. Express* **25** 26792
[4] McCaughan A N, Zhai Y, Korzh B, Allmaras J P, Oripov B G, Shaw M D and Nam S W 2022 The thermally coupled imager: a scalable readout architecture for superconducting nanowire single photon detectors *Appl. Phys. Lett.* **121** 102602
[5] Nihei M, Kawabata A, Kondo D, Horibe M, Sato S and Awano Y 2005 Electrical properties of carbon nanotube bundles for future via interconnects *Jpn. J. Appl. Phys.* **44** 1626
[6] Hone J, Llaguno M C, Biercuk M J, Johnson A T, Batlogg B, Benes Z and Fischer J E 2002 Thermal properties of carbon nanotubes and nanotube-based materials *Appl. Phys.* A **74** 339–43
[7] Zubair A, Tsentalovich D E, Young C C, Heimbeck M S, Everitt H O, Pasquali M and Kono J 2016 Carbon nanotube fiber terahertz polarizer *Appl. Phys. Lett.* **108** 141107
[8] Zubair A, Wang X, Mirri F, Tsentalovich D E, Fujimura N, Suzuki D, Soundarapandian K P, Kawano Y, Pasquali M and Kono J 2018 Carbon nanotube woven textile photodetector *Phys. Rev. Mater.* **2** 015201
[9] Tomlin N A *et al* 2020 Overview of microfabricated bolometers with vertically aligned carbon nanotube absorbers *AIP Adv.* **10** 055010
[10] Yang Z-P, Ci L, Bur J A, Lin S-Y and Ajayan P M 2008 Experimental observation of an extremely dark material made by a low-density nanotube array *Nano Lett.* **8** 446–51
[11] Chunnilall C J, Lehman J H, Theocharous E and Sanders A 2012 Infrared hemispherical reflectance of carbon nanotube mats and arrays in the 5–50μm wavelength region *Carbon* **50** 5348–50
[12] Yung C S, Tomlin N A, Heuerman K, Keller M W, White M G, Stephens M and Lehman J H 2018 Plasma modification of vertically aligned carbon nanotubes: superhydrophobic surfaces with ultra-low reflectance *Carbon* **127** 195–201
[13] Dresselhaus M S, Dresselhaus G, Saito R and Jorio A 2007 Exciton photophysics of carbon nanotubes *Annu. Rev. Phys. Chem.* **58** 719–47
[14] Perebeinos V, Tersoff J and Avouris P 2005 Effect of exciton-phonon coupling in the calculated optical absorption of carbon nanotubes *Phys. Rev. Lett.* **94** 027402
[15] Murakami Y, Lu B, Kazaoui S, Minami N, Okubo T and Maruyama S 2009 Photoluminescence sidebands of carbon nanotubes below the bright singlet excitonic levels *Phys. Rev.* B **79** 195407
[16] Allmaras J P, Kozorezov A G, Korzh B A, Berggren K K and Shaw M D 2019 Intrinsic timing jitter and latency in superconducting nanowire single-photon detectors *Phys. Rev. Appl.* **11** 1
[17] Verma V B, Lita A E, Stevens M J, Mirin R P and Nam S W 2016 Athermal avalanche in bilayer superconducting nanowire single-photon detectors *Appl. Phys. Lett.* **108** 131108
[18] Allmaras J P, Wollman E E, Beyer A D, Briggs R M, Korzh B A, Bumble B and Shaw M D 2020 Demonstration of a thermally coupled row-column SNSPD imaging array *Nano Lett.* **20** 2163–8
[19] McCaughan A N, Verma V B, Buckley S M, Allmaras J P, Kozorezov A G, Tait A N, Nam S W and Shainline J M 2019 A superconducting thermal switch with ultrahigh impedance for interfacing superconductors to semiconductors *Nat. Electron.* **2** 451–6
[20] Brunel M, Enzo S, Jergel M, Luby S, Majkova E and Vavra I 1993 Structural characterization and thermal stability of W/Si multilayers *J. Mater. Res.* **8** 2600–7
[21] Deneuville A, Benyahya M, Brunel M and Canut B 1988 Influence of the annealing atmosphere on the chemical and thermal stability of amorphous WSi_2 *J. Less-Common Met.* **145** 197–207
[22] Young B A, Saab T, Cabrera B, Cross J J, Clarke R M and Abusaidi R A 1999 Measurement of T_c suppression in tungsten using magnetic impurities *J. Appl. Phys.* **86** 6975–8
[23] McCaughan A N, Tait A N, Buckley S M, Oh D M, Chiles J T, Shainline J M and Woo Nam S 2021 PHIDL: Python-based layout and geometry creation for nanolithography *J. Vac. Sci. Technol.* B **39** 062601
[24] Kumanek B and Janas D 2019 Thermal conductivity of carbon nanotube networks: a review *J. Mater. Sci.* **54** 7397–427
[25] Chen G 1967 On the physics of purple-plague formation and the observation of purple plague in ultrasonically-joined gold-aluminum bonds *IEEE Trans. Parts Mater. Packag.* **3** 149–53